Journal of Structural Geology 34 (2012) 30–42

Contents lists available at SciVerse ScienceDirect

Journal of Structural Geology

journal homepage: www.elsevier.com/locate/jsg

Analysis of superposed strain: A case study from Barr Conglomerate in the South Delhi Fold Belt, Rajasthan, India

Nilanjan Dasgupta [a,*], Dhruba Mukhopadhyay [b], T. Bhattacharyya [c]

[a] Department of Geology, Presidency University, 86/1 College Street, Kolkata 700073, West Bengal, India
[b] Raman Centre for Applied and Interdisciplinary Sciences, Kolkata 700032, West Bengal, India
[c] Department of Geology, University of Calcutta, 35 Ballygunge Circular Road, Kolkata 700019, West Bengal, India

ARTICLE INFO

Article history:
Received 28 May 2011
Received in revised form
24 October 2011
Accepted 31 October 2011
Available online 10 November 2011

Keywords:
Strain analysis
Strain superposition
Strain factorization
Pebble deformation
Barr conglomerate

ABSTRACT

The structural geometry in the Barr conglomerate and the neighboring rocks in the western flank of the Meso- to Neoproterozoic South Delhi Fold Belt indicate superposed deformation, with structures developed by horizontal dextral simple shear deformation superimposed on earlier structures formed during approximately ESE-WNW compression and subvertical maximum elongation. The first deformation produced NNE-SSW trending subvertical schistosity, and associated steeply plunging isoclinal folds, mineral lineation and pebble elongation lineation having almost downdip alignment on the schistosity surface. The second deformation produced dextral folds both on bedding and schistosity surfaces and modified the shape of the pebbles already deformed by the first deformation. On vertical sections perpendicular to the schistosity trace the pebbles show sub-ellipsoidal shape with their mean elongation direction parallel to the schistosity trace. On the horizontal section the pebbles often show asymmetrical shape and asymmetrical deflection of the schistosity surface around the pebbles. The mean elongation direction makes a small angle (2°–8°) in the counter-clockwise sense with the schistosity surface. This obliquity is due to modification of post-first-deformation sub-ellipsoidal shape by later horizontal simple shear using the schistosity surface as the movement plane. Analytical expressions are derived for the modification of an original ellipse by simple shear parallel to the long axis of the ellipse. A family of curves has been generated to depict the change in axial ratio and orientation of long axis for different initial axial ratios, and for different values of shear strain (γ). Using these curves it has been possible to factorize the total strain into two components representing the earlier compression and the later simple shear. It is noted that the computed earlier shortening strain ellipsoids are consistently in the flattening field close to the line of pure oblate ellipsoids in the Flinn plot. There is no systematic spatial control on the variation in the values of shear strain (γ), strain ellipsoid shape parameter (k), and intensity of distortion (d) as one proceeds south to north along the strike of the conglomerate.

1. Introduction

Pebble shapes in deformed conglomerates have long been used to estimate finite strain in rocks. If the pebbles were all initially spherical and had the same viscosity as the matrix, they would behave as passive markers, and the pebble shape after deformation would represent the strain ellipsoid. On the other hand, if the initial shapes of the pebbles were ellipsoidal, their final shapes would not represent the strain ellipsoid but would depend upon the finite strain and the initial shape and orientation of the pebble. The basic principle of strain measurement from initial non-spherical markers was first discussed by Ramsay (1967). This led to a method, known as the R_f-φ method, that was later elaborated by several workers (Dunnet, 1969; Ramsay and Huber, 1983; Lisle, 1985; and references therein). Graphical and algebraic methods have been devised to compute the shape of finite strain ellipse from measurement of shapes of deformed pebbles that were initially elliptical (De Paor, 1988; Dunnet, 1969; Dunnet and Siddans, 1971; Elliott, 1970; Gay, 1968a,b; Holst, 1982; Lisle, 1977; Mukhopadhyay and Bhattacharya, 1969; Oertel, 1978; Shimamoto and Ikeda, 1976; Wheeler, 1984). The hyperbolic net of De Paor (1988) provides a handy method for estimating the strain ratio and orientation of the strain ellipse using the principle of R_f-φ method. Shimamoto and Ikeda (1976) proposed an algebraic method of strain analysis from a population of deformed elliptical markers. This method is

* Corresponding author.
E-mail address: neelakdg@gmail.com (N. Dasgupta).

0191-8141/$ – see front matter © 2011 Elsevier Ltd. All rights reserved.
doi:10.1016/j.jsg.2011.10.010

more objective than the graphical R_f-φ method. The R_f-φ method is suitable for pebbles having ideally random orientations though a number of authors including Elliott (1970), Dunnet and Siddans (1971) and Lisle (1985) have discussed methods to tackle the problem of initial pebble fabric.

Two other aspects which are important in this context are viscosity contrast between pebbles and matrix and pebble concentration (Bilby et al., 1975; Freeman, 1987; Gay, 1968a,b, 1969; Gay and Fripp, 1976; Mandal et al., 2003; Vitale and Mazzoli, 2005). Bilby et al. (1975) and Gay (1968a) showed that for isolated more competent circular or elliptical objects in a matrix the object strain ratio is less than the bulk strain ratio and their difference is a function of the viscosity contrast. For two-dimensional strain they presented equations linking the bulk strain ratio with the object strain ratio and the viscosity contrast. Numerically solving the Eshelby–Bilby equations Freeman (1987) showed that objects more competent than the matrix will have deformed shapes with larger *k*-values (Flinn, 1962) than equivalently shaped and oriented passive markers, and the effect increases with increasing viscosity ratio. Treagus and Treagus (2001) further showed that competent elliptical objects with axial ratios of 3 or more will strain more than circular objects of the same viscosity, and if the objects are incompetent they will strain less. Such effect would be insignificant for competent objects with axial ratio of less than 2. The data compiled by Lisle (1985), however, show that most undeformed conglomerates have initial axial ratios in the range of 1.5–2. Such pebbles would strain only marginally more that circular objects of same viscosity.

The conclusions of the workers mentioned above apply to isolated objects in a matrix where an individual object is not influenced by the surrounding ones. Gay (1968a) showed that in a multi-object system the number and the volume of the objects relative to the matrix have a bearing on the effective viscosity. He coined the term "effective mean viscosity ratio" (R_m) that would control the bulk strain of the rock and gave a mathematical expression for it. He noted that R_m rapidly decreases with increasing object concentration and approaches the value of 1 in a densely packed system. Numerical analysis by Mandal et al. (2003) also reveals that the ratio of the object to the bulk strain rate increases non-linearly with greater packing density. For competent objects the object strain rate is less than the bulk strain rate and both approach the same value for high object concentration. Working with naturally deformed rocksVitale and Mazzoli (2005) showed that in a multi-object system the measured finite strain for competent objects is less than that for the bulk rock, and the effective (measured) finite strains for both bulk rock and objects and the effective viscosity ratio are all less than the corresponding values in case of isolated objects with no particle interaction. Further, the measured values of object strain, bulk strain and effective viscosity ratio decrease rapidly with increasing object concentration. The ratio of effective bulk strain to object strain and the viscosity ratio both approach the value of 1 for maximum packing. Thus theoretical and observational data from a number of workers indicate that a high concentration of pebbles, even with large viscosity contrast, would bring the effective mean viscosity ratio close to 1, implying that the pebble strain would be the same as the bulk strain. In the present study the average concentration of

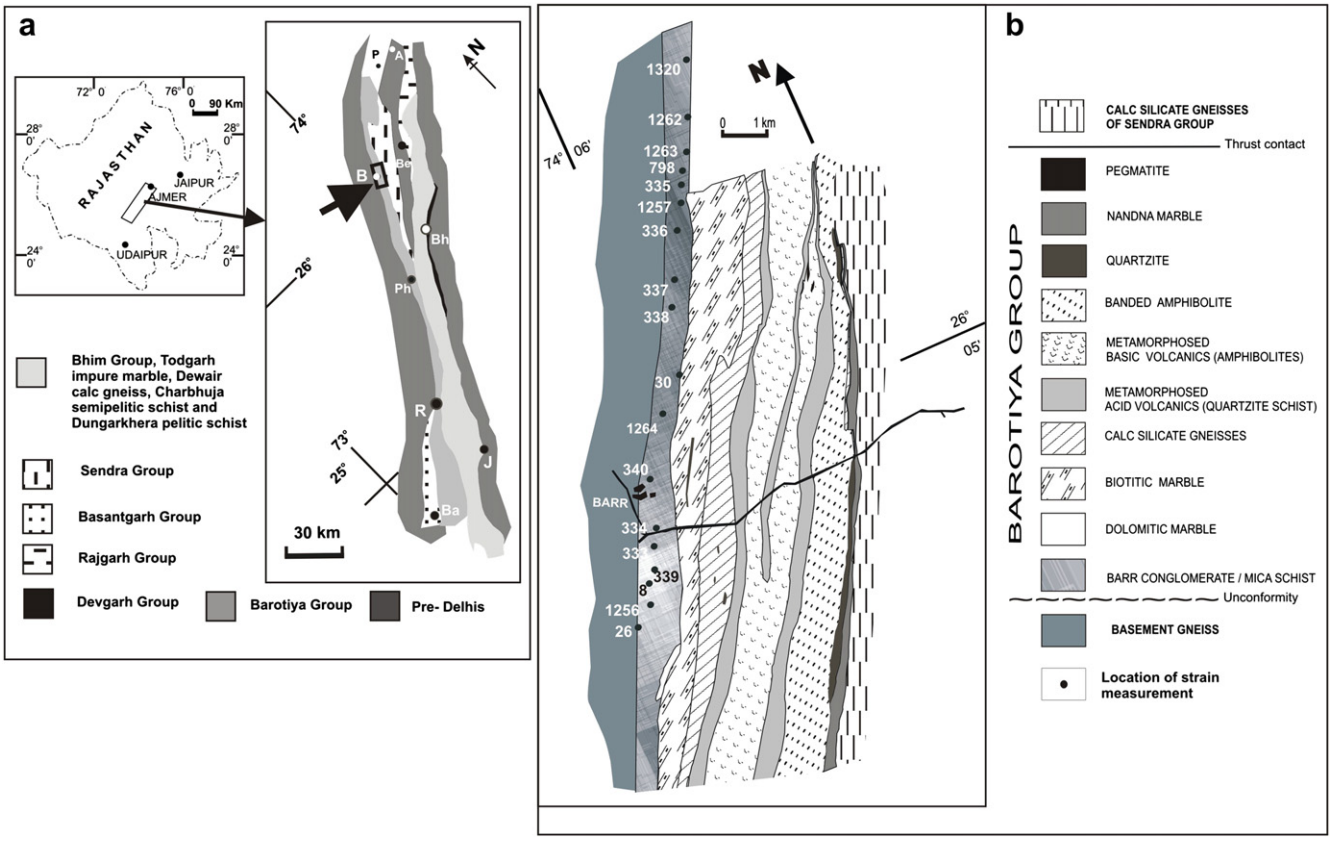

Fig. 1. a. General geological map of South Delhi Fold Belt (redrawn after Gupta and Bose, 2000). Inset shows geographic location of South Delhi Fold Belt. P: Pushkar, A: Ajmer, B: Barr, Be: Beawar, Ph: Phulad, Bh: Bhim, R: Ranakpur, J: Jaswantgarh, Ba: Basantgarh. b. Lithological map of the area (marked by arrow in Fig. 1a) showing the locations of samples for strain analysis.

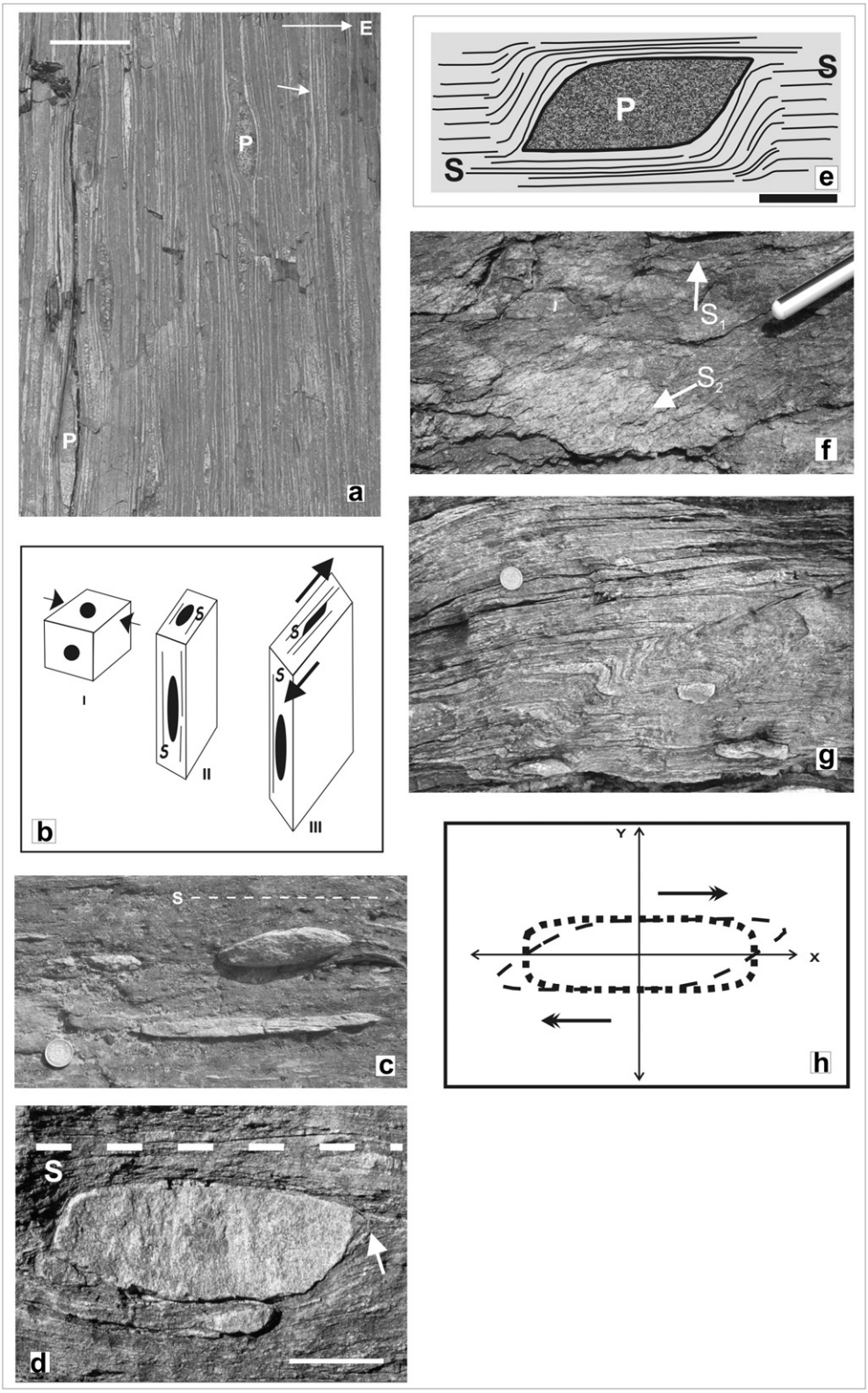

Fig. 2. In the sketches and photographs *P*, and *S* represent pebble and schistosity respectively. a. Vertical section of Barr Conglomerate facing south showing thin streaks(shown by arrow) of quartzo-feldspathic materials (could represent disrupted primary layering), giving a banded appearance. The long axes of pebbles are parallel to the trace of the schistosity in this section. Scale bar is twelve inches. b. Cartoon showing the strain evolution in the area. I - Initial stage, II - After irrotational orthogonal extension-contraction (D_1); development of subvertical schistosity, and downdip elongation lineation, III - After sub-horizontal dextral simple shear (D_2); ellipse modified on YZ plane, no change in vertical direction. c. Long axes of pebbles oriented oblique to the trace of the schistosity in a counter-clockwise sense (horizontal surface, YZ plane). Diameter of the coin is 2.3 cm. d. Pebble with two diagonally opposite angular corners, other two corners being rounded. Note asymmetric deflection of schistosity around the pebble. Scale bar is 6 cm. e. Sketch of pebble with shape as shown in Fig. 2d. Note asymmetric deflection of schistosity round the pebble. f. Foliated granite pebble seen on plan. Note the irregular boundary of the pebble. Main schistosity (S_1) is cut across by a spaced cleavage (S_2). g. Flattened pebble and foliation in matrix dextrally kinked. Towards right the kink passes into a series of en echelon cracks almost parallel to the axial plane of the kink folds. Diameter of the coin is 2.3 cm. h. Superellipse (dotted line) with $n = 4.0$, axial ratio $= 2.5$. Dextral simple shear ($\gamma = 2.5$) gives rise to asymmetric shape as in Fig. 2 d, e.

the pebbles that have been used for strain analysis is about 40% by volume. From the graph of Gay (1968a, Fig. 10), R_m of such a pebble-matrix system would be close to 1. Therefore, the object strain computed in this study closely approximates the bulk strain.

Another important conclusion of the above studies is that though in such a system the strain in the matrix surrounding the objects is heterogeneous, the objects themselves deform homogeneously if they have circular or elliptical shape and are not closely packed (Treagus and Treagus, 2001). Closely packed objects would be heterogeneously strained; isolated non-elliptical objects would also deform heterogeneously (Treagus and Lan, 2003; 2004). In our analysis we have assumed that in general the pebbles have deformed homogeneously.

In superposed deformation if the successive strains are all homogeneous the final strain would also be homogeneous and would be represented by a single strain ellipsoid (Ramsay, 1967). If only the final strain ellipsoid is known, to separate the strains resulting from each deformation is a difficult and often an impossible task. Here we discuss the special situation of superposition of simple shear on pure shear and attempt to compute the two different strains from measurements on deformed pebbles in a conglomerate.

2. Deformation pattern

The Barr Conglomerate, which is the subject of this study, occurs along the western margin of the Meso- to Neoproterozoic South Delhi Fold Belt (SDFB) in Rajasthan, western India. It is the basal unit of the Barotiya Group (within the Delhi Supergroup), which overlies the basement of Banded Gneissic Complex (BGC) exposed to its west (Heron, 1953; Gupta and Bose, 2000) (Fig. 1). This contact has been referred to as a strong deformation/shear zone (Ghosh et al., 1999; Sen, 1980; 1981; Sengupta and Ghosh, 2004; 2007).

A structural study in the rocks of the Barotiya Group indicates the presence of three deformational phases (Dasgupta, 2010). The first deformation episode (D_1) produced long-limbed isoclinal folds with axial planar schistosity or gneissosity which became asymmetrically folded with dextral vergence (Z-shaped folds) during the second deformation phase (D_2). Thin streaks of quartzo-feldspathic material parallel to schistosity in the conglomerate probably represent disrupted primary layers (Fig. 2a); bedding in the associated calc-gneiss and the major lithological contacts are parallel to the D_1 schistosity (S_1) due to isoclinal nature of the folds. The last phase D_3 is weak and has produced broad warps of schistosity and bedding on transverse east-west axial planes. Details of the structural geometry will be described elsewhere; here we only mention that the sense of shear has been worked out from (a) σ-structures around feldspar porphyroclasts in the acid volcanics, (b) mica fish in the mylonitic rocks, (c) S–C fabrics in local shear zones, and (d) elongation of small quartz grains oblique to the main schistosity which acted as the movement planes in mylonitic quartzites. We interpret that earlier (D_1) irrotational orthogonal extension-contraction (pure shear) was followed by horizontal dextral simple shear (D_2) (Fig. 2b). The combination of irrotational orthogonal extension-contraction and simple shear is analogous to transpression, but here the two are not simultaneous. Superposition of simple shear on earlier irrotational orthogonal extension-contraction strain is indicated by the refolding of isoclinal folds by later asymmetrical (dextral) folds and dextral folding of the D_1 schistosity (S_1) and development of D_2 crenulation cleavage or spaced cleavage (S_2). Moreover, in calc-gneisses, the D_2 planar fabric (S_2) is defined by later biotite flakes cutting across older amphibole and pyroxene grains defining the D_1 gneissosity.

Initial irrotational orthogonal extension-contraction followed by sub-horizontal dextral simple shear is also reflected in the pebble shapes of the Barr Conglomerate. The maximum elongation of the pebbles on the schistosity surface is nearly downdip. On vertical sections perpendicular to the schistosity the pebbles are sub-ellipsoidal, and the mean orientation of the long axes is parallel to the schistosity trace indicating schistosity normal compression (Fig. 2a). The effect of sub-horizontal dextral simple shear is seen on the horizontal surface. The features indicative of this shear are, (i) alignment of mean orientation of long axes of elliptical pebbles oblique to the schistosity trace in a counter-clockwise sense (Fig. 2c), (ii) asymmetric deflection of schistosity trace in the matrix around the pebbles (Fig. 2d and e), (iii) oblique s-plane formed in local shear zones cutting across flattened elliptical pebbles (Fig. 2f) and (iv) dextral kinking of elliptical pebbles and schistosity within the conglomerate (Fig. 2g).

Some pebbles in the Barr Conglomerate have a distinctive shape characterized by an asymmetry with two diagonally opposite angular corners, the two other corners being rounded (Fig. 2d, e). Treagus and Lan (2000, 2003) have shown that similar shapes are developed in incompetent objects in both pure shear and simple shear if the initial shapes are squares with their sides askew to either the elongation and shortening directions (pure shear) or the shear direction (simple shear). Their model is not applicable in the present case because the quartzite pebbles are expected to be more competent than the micaceous schistose matrix. We propose that this shape was formed by simple shear deforming an initial superellipse (Gardner, 1965; Lisle, 1988) formed by earlier pure shear. A superellipse has the general formula, $(x/a)^n + (y/b)^n = 1$. Where n is >2, the shape is a rectangle with rounded corners. Fig. 2h illustrates a superellipse ($n = 4$) deformed by simple shear with movement direction parallel to x-axis ($\gamma = 2.5$). The resultant shape has the characteristic angular and rounded corners.

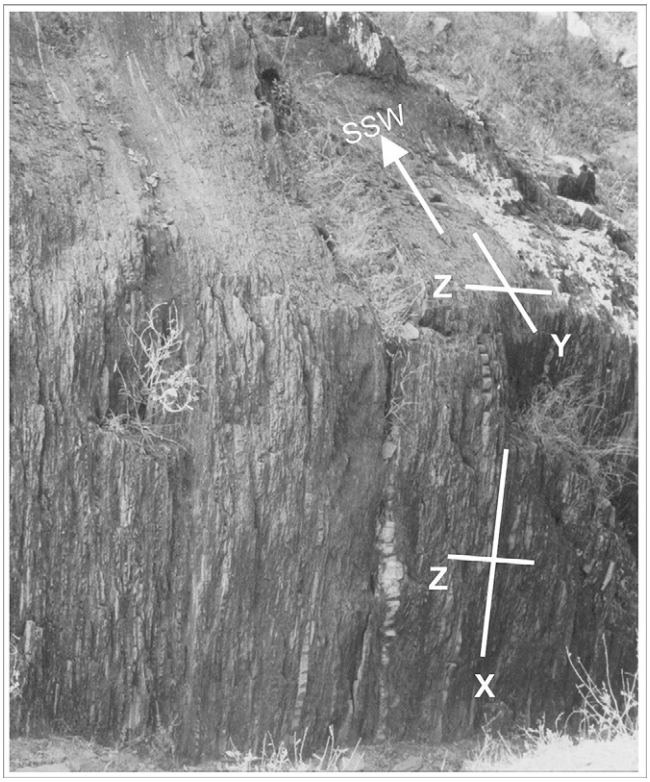

Fig. 3. Outcrop of Barr Conglomerate south of Barr viewed from north. The schistosity plane is the XY plane of the first phase strain ellipsoid. Two planes of measurement are the vertical and the horizontal sections, which represent the XZ and YZ planes of the first phase strain ellipsoid.

Table 1
Pebble shape (axial ratio) and orientation of long axes on the vertical plane (XZ plane) of measurement, at different locations. Angle of long axis of pebble is measured with respect to trace of schistosity. Counter-clockwise angle is positive.

Location number	Sample size	Axial ratio						Orientation of long axis (with respect to the schistosity trace on the section)		
		$R_f - \phi$ Method (De Paor, 1988)	Harmonic mean	Std. deviation	Geometric mean	Std. deviation	Linear correlation	Vector mean	Std. deviation	ϕ (De Paor, 1988)
333	17	8.0	9.07	0.43	12.45	0.84	9.03	−0.65	0.23	0
334	30	5.5	6.47	0.10	7.98	0.70	5.95	−0.67	0.18	0.5
335	51	7.0	9.69	1.49	12.50	0.77	12.15	1.35	0.30	0
336	36	6.0	6.57	0.08	7.75	0.62	7.85	−0.05	0.35	0
337	27	6.0	6.38	0.10	7.89	0.69	6.68	−0.41	0.32	0
338	16	10.0	9.14	0.07	10.77	0.57	7.72	0.56	0.04	0.5
339	32	10.0	13.32	0.04	15.61	0.60	12.38	−0.59	0.02	0
340	26	5.7	6.53	0.06	7.00	0.37	7.51	−0.73	0.05	0
798	48	6.0	6.70	0.10	8.02	0.62	6.59	1.23	0.06	2
1256	34	7.0	5.91	0.13	7.51	0.70	7.49	−0.23	0.04	0
1257	28	4.6	4.84	0.12	5.67	0.60	6.37	0.39	0.02	0
1262	31	5.5	5.58	0.14	6.79	0.61	5.62	−0.10	0.04	0
1263	29	5.5	6.46	0.11	8.11	0.71	7.87	0.00	0.00	0
1264	31	6.0	5.73	0.10	6.83	0.63	5.79	−0.13	0.01	0
1320	30	5.5	5.45	0.13	6.66	0.66	5.37	0.57	0.04	0
8	23	2.2	4.42	0.08	4.64	0.31	4.40	−1.57	0.06	0
26	15	2.4	5.74	0.07	6.18	0.39	6.40	0.52	0.09	0
30	18	6.0	8.52	0.06	9.60	0.51	7.13	4.17	0.07	4

3. Pebble measurements

Measurements of pebbles have been carried out at 18 locations spread throughout the strike-length of the conglomerate band extending over a distance of 13 km (Fig. 1b). The subvertical schistosity plane is considered to be the XY plane of strain ellipsoid of the first deformation (Ramsay and Huber, 1983; p. 184). The mean orientation of the long axes of the pebbles on the schistosity plane is considered to be the *X*-direction of this strain ellipsoid, and is nearly down dip on the schistosity plane (Fig. 3). The *Y* and *Z* directions are nearly horizontal, parallel and perpendicular to the schistosity trace. The sub-horizontal shear used the schistosity surface as the movement plane and the above mentioned *Y*-direction was the movement direction. This simple shear does not have any effect in the *X*-direction, but the directions of *Y* and *Z* of the final ellipsoid change slightly. The angle between the *Z*-direction of the first ellipsoid and the *Z*-direction of the final ellipsoid is very small, and as a first approximation the XZ planes of both the first and final ellipsoids are taken to be the vertical plane.

Measurements for strain analysis were done on horizontal planes (YZ plane of first and final ellipsoids) and on vertical joint planes perpendicular to schistosity (XZ plane of first and final ellipsoids) (Fig. 3). The 2-dimensional strain ratios were combined to calculate the 3-dimensional strain.

Only the quartzite pebbles were used for strain analysis for the following reasons:

a) These are the most common pebbles and outnumber the granitic pebbles in any outcrop seen within the area.
b) The sharp boundaries of the quartzite pebbles make it easier to measure them than the foliated granite pebbles with fuzzy boundaries (Fig. 2f).
c) The range of size variation of the quartzite pebbles is large, which ensures that the analysis has been done on a wide size

Table 2
Pebble shape (axial ratio) and orientation of long axis for the horizontal plane (YZ plane) of measurement, at different locations. Angle of long axis of pebble is measured with respect to trace of schistosity. Counter-clockwise angle is positive.

Location number	Sample size	Axial ratio						Orientation of long axis (with respect to the schistosity trace on the section)		
		$R_f - \phi$ method (De Paor, 1988)	Harmonic mean	Std. deviation	Geometric mean	Std. deviation	Linear correlation	Vector mean	Std. deviation	ϕ (De Paor, 1988)
333	29	4.6	4.97	0.07	4.92	0.36	4.54	3.72	0.06	4
334	49	4.8	4.06	0.16	4.84	0.60	4.96	3.27	0.20	5
335	27	4.6	5.09	0.09	5.74	0.53	4.48	6.52	0.04	10
336	32	6.5	6.28	0.05	6.60	0.32	6.48	5.62	0.33	5
337	25	6.5	6.23	0.07	6.87	0.48	5.33	3.20	0.37	3
338	45	6.0	5.96	0.09	6.75	0.50	4.93	2.13	0.21	2
339	37	6.5	6.98	0.07	7.83	0.49	6.41	1.95	0.06	0
340	39	6.8	7.42	0.05	8.12	0.41	7.11	3.26	0.06	4
798	49	5.0	4.66	0.12	5.48	0.62	3.63	4.20	0.05	5
1256	34	5.5	5.06	0.10	5.72	0.51	5.53	1.35	0.06	0
1257	34	4.4	4.51	0.14	5.57	0.67	4.91	2.73	0.05	4
1262	39	4.8	4.55	0.13	5.30	0.57	3.35	4.77	0.06	4
1263	39	5.2	5.26	0.09	5.87	0.52	4.62	3.97	0.06	4
1264	25	4.0	4.81	0.09	5.34	0.49	3.72	4.44	0.07	5
1320	38	5.0	4.06	0.14	4.67	0.53	4.85	2.08	0.07	5
8	41	2.4	2.86	0.13	3.05	0.37	2.77	0.70	0.13	2
26	38	2.7	4.24	0.07	4.45	0.32	4.54	4.93	0.07	5
30	40	3.8	4.98	0.11	5.68	0.53	5.05	7.28	0.09	10

Table 3
Harmonic mean and orientation of long axis for the horizontal plane (YZ plane) and vertical plane (XZ plane) of measurement, at different locations.

Location number	Horizontal plane					Vertical plane				
	No. of data	Axial ratio		Orientation of long axis (with respect to the cleavage on the section)		No. of data	Axial ratio		Orientation of long axis (with respect to the cleavage on the section)	
		Harmonic mean	Std. dvn.	Vector mean	Std. dvn.		Harmonic mean	Std. dvn.	Vector mean	Std. dvn.
333	29	4.97	0.07	3.72	0.26	17	9.07	0.43	−0.65	0.23
334	49	4.06	0.16	3.27	0.20	30	6.47	0.10	−0.67	0.18
335	27	5.09	0.09	6.52	0.04	51	9.69	1.49	1.35	0.30
336	32	6.28	0.05	5.62	0.33	36	6.57	0.08	−0.05	0.35
337	25	6.23	0.07	3.20	0.37	27	6.38	0.10	−0.41	0.32
338	45	5.96	0.09	2.13	0.21	16	9.14	0.07	0.56	0.04
339	37	6.98	0.07	1.95	0.06	32	13.32	0.04	−0.59	0.02
340	39	7.42	0.05	3.26	0.06	26	6.53	0.06	−0.73	0.05
798	49	4.66	0.12	4.20	0.05	48	6.70	0.10	1.23	0.06
1256	34	5.06	0.10	1.35	0.06	34	5.91	0.13	−0.23	0.04
1257	34	4.51	0.14	2.73	0.05	28	4.84	0.12	0.39	0.02
1262	39	4.55	0.13	4.77	0.06	31	5.58	0.14	−0.10	0.04
1263	39	5.26	0.09	3.97	0.06	29	6.46	0.11	0.00	0.00
1264	25	4.81	0.09	4.44	0.07	31	5.73	0.10	−0.13	0.01
1320	38	4.06	0.14	2.08	0.07	30	5.45	0.13	0.57	0.04
8	41	2.86	0.13	0.70	0.13	23	4.42	0.08	−1.57	0.06
26	38	4.24	0.07	4.93	0.07	15	5.74	0.07	0.52	0.09
30	40	4.98	0.11	7.28	0.09	18	8.52	0.06	4.17	0.07

range, thereby negating any bias on size dependency of the analysis.

During the site selection and collection of data the following points were taken into consideration:

a) Pebbles within an area of generally 2 m × 2 m were measured.
b) It was ensured that the pebbles did not impinge upon one another.
c) Data were collected from places where the schistosity was overall planar and unfolded.

The principal parameters which were measured for each individual pebble were,

i. Lengths of long and short axes of each pebble
ii. Orientation (ϕ) of long axis with respect to the schistosity trace. A counter-clockwise angle (dextral asymmetry) from the schistosity trace is taken to be positive, while a clockwise angle (sinistral asymmetry) is taken to be negative.

Other parameters which were measured include,

i. The areal density of the pebbles over the area of measurement, usually from the photographs of the planes of measurement.
ii. The attitude of the pebble long axis lineation on the schistosity surface.
iii. The attitude of the schistosity.
iv. The attitudes of the two planes of measurement.

In this paper we present the summary data processed from the raw data collected in the field. The raw data are available on request from the first author.

4. Methodology for calculating the strain ratio

The data collected from the two perpendicular measurement sections at each location were treated separately to compute the 2–dimensional strain ratio. The results obtained are presented in Tables 1, 2 and 3. A preliminary estimate of the axial ratio and the orientation of the two-dimensional strain ellipse was calculated by R_f-ϕ method using De Paor's net for both the measurement surfaces (Fig. 4).

It is observed that each population has a fairly large range of R_f values but a very narrow range of ϕ values. The axial ratios of the deformed pebbles on the YZ section have a much larger range than on the XZ section. The mean angle made by the long axis of the pebbles with the schistosity trace (ϕ) is non-zero in anticlockwise sense (maximum of 14°) on the YZ section and is almost 0° on the

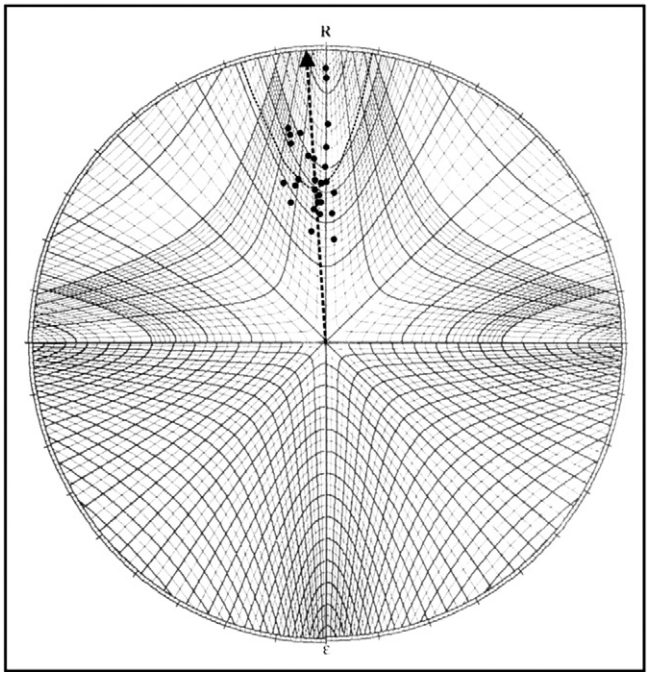

Fig. 4. Representative plot of axial ratio versus orientation of long axis of the pebbles of the sub-horizontal plane at location 333 on the hyperbolic net of De Paor (1988). Reference line *R* represents trace of schistosity. Note that the symmetry line (represented by arrow) is not parallel to trace of the schistosity.

XZ section. On the vertical (XZ) plane, the vector mean of the pebble long axes is parallel to the schistosity trace and the standard deviation around the vector mean angle is very small (Fig. 5); the fluctuation of the pebble long axes is also small (maximum 7°). The vector mean of the pebble long axes on the YZ plane is not parallel to the schistosity trace. The test of symmetry does not hold good in this case. Because of the above reasons, we conclude that the R_f-ϕ method may not be appropriate for strain determination.

We adopted a statistical approach of determining the axial ratio and the orientation of the two-dimensional ellipse which would also test the accuracy of the results obtained by R_f-ϕ method. Our objective was to characterize the pebble population on each measurement plane with an average axial ratio and an average orientation of long axis, and use these for estimating the strain parameters.

The average orientation of the long axes is given by the vector mean of the angles between the pebble long axis and the trace of the schistosity. Three estimates of the average axial ratio that are determined are harmonic mean, geometric mean (Lisle, 1977) and the slope of the best fit line on x-y plot employing the method of linear correlation (Mukhopadhyay, 1973). The results are presented in Tables 1, 2 and 3.

Lisle (1977) estimated the finite strain ellipse from the arithmetic, geometric and harmonic means of the axial ratios of the individual synthetically deformed elliptical markers in a population. He discussed two mathematical models (uniform and random mode), in which he considered suites of elliptical markers of known initial axial ratio deformed by pure shear yielding a final axial ratio. He observed that none of the means exactly represents the strain ellipse. According to him, the harmonic mean is the closest approximation to the strain ellipse, followed by the geometric mean.

In the present study, it is observed that for a given population the geometric mean is greater than the harmonic mean; and the ratio determined by the linear correlation method is close to the harmonic mean, at places slightly greater than and at places slightly less than the harmonic mean. Following Lisle (1977) we have used the harmonic mean as the best estimate of the axial ratio of the final ellipse derived from an initial circle, which would give the two-dimensional strain ratio ($\sqrt{\lambda_1/\lambda_2}$).

5. Discussion of the results obtained

5.1. Finite strain ellipse on XZ plane (Table 1)

The vector mean of the orientation of long axes of the pebbles with respect to the trace of the schistosity on the plane of measurement varies from −1.57° to +1.35° (standard deviation

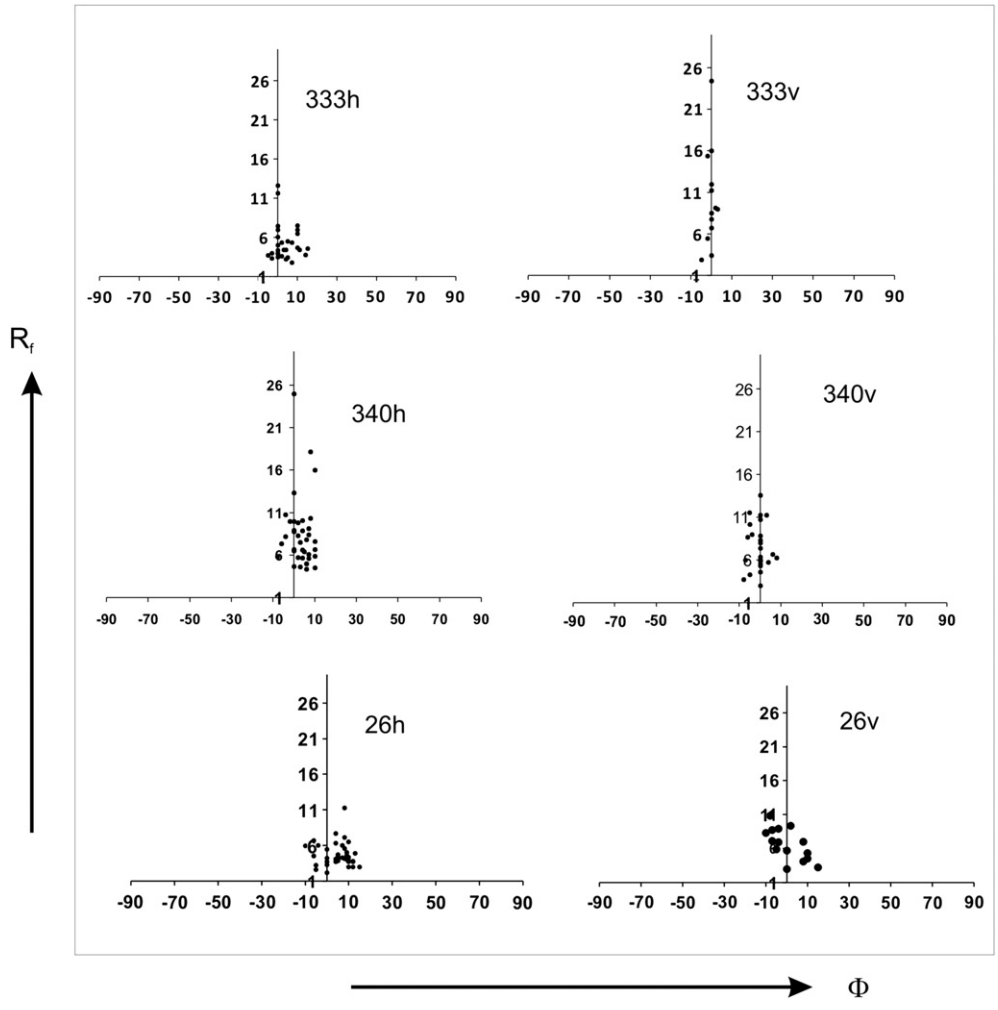

Fig. 5. Representative plots of axial ratio versus orientation of long axis of the pebbles for three different locations, namely 333, 340 and 26. '*h*' denotes the horizontal plane of measurement, '*v*' denotes the vertical plane of measurement. The schistosity trace is represented by the 0^0 line. Note that on vertical plane data are symmetrically distributed on either side of schistosity, while on horizontal plane symmetry line is not parallel to schistosity trace.

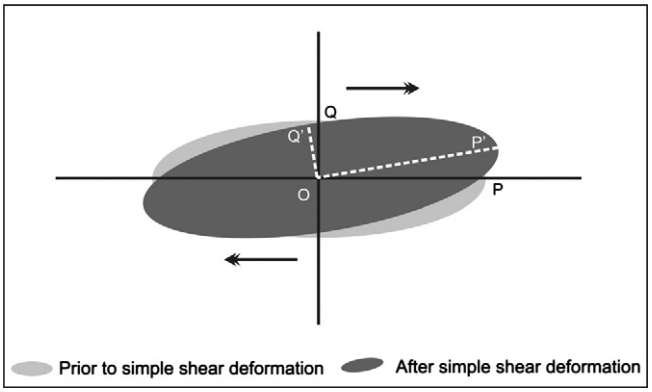

Fig. 6. Deformation of an initial ellipse by shearing in a direction parallel to x-coordinate axis produces another ellipse. OP and OQ are the semi major and minor axes of the initial ellipse. OP' and OQ' are the semi major and minor axes of the deformed ellipse (see text for details).

ranging from 0° to 0.32°) excepting location #30 where the angle is >4° and is quite different from the rest. Hence for all practical purposes the mean long axis can be considered to be parallel to the trace of the schistosity. This can be taken to represent the orientation of the long axis of the final strain ellipse with a reasonable degree of certainty (Ramsay, 1967; Ramsay and Huber, 1983). The harmonic means at different localities vary from 4.42 to 13.32. At each locality the standard deviation is small, generally of the order of ~0.1. The true axial ratio of the strain ellipse is considered to lie within the ±2 σ interval around the harmonic mean at 95% confidence interval (Lisle, 1977).

5.2. Finite strain ellipse on YZ plane (Table 2)

On this plane of measurement the average fluctuation of the orientation of long axes of the pebbles is 18° and ranges from 7° to 30° with only one location (#8) having a fluctuation of 45°. The vector means always make a counter-clockwise angle with the schistosity trace (0°), and the angles vary from 1.35° to 7.28° (barring 0.7° at #8, which is quite dissimilar from the rest of the locations).

The harmonic means vary from 2.86 to 7.42. The standard deviation at each location is of the order of ~0.1. The harmonic mean (representing the strain ratio) and the vector mean (representing the orientation of long axis of the final strain ellipse) for the two measurement planes for all locations have been listed in Table 3.

6. Analysis of superposed strain

Any finite strain may be represented by a deformation matrix and the orientation and geometry of strain ellipsoid may be calculated from the components of the deformation matrix (Ramsay and Huber, 1983). Irrotational orthogonal extension-contraction, simple shear, rotation etc. are specific deformation types characterized by specific forms of deformation matrix. Any finite deformation matrix can be factorized in an infinite number of ways into two or more deformation matrices, each representing a particular deformation occurring in a particular sequence. A common factorization is decomposition into irrotational orthogonal extension-contraction, and simple shear, with or without dilation. The following equation gives three possible ways of factorizing a given 2-D deformation matrix (D) (Fossen and Tikoff, 1993; Tikoff and Fossen, 1993).

$$D = \begin{bmatrix} k_1 & 0 \\ 0 & k_2 \end{bmatrix}\begin{bmatrix} 1 & \gamma_{s,p} \\ 0 & 1 \end{bmatrix} = \begin{bmatrix} 1 & \gamma_{p,s} \\ 0 & 1 \end{bmatrix}\begin{bmatrix} k_1 & 0 \\ 0 & k_2 \end{bmatrix} = \begin{bmatrix} k_1 & \Gamma \\ 0 & k_2 \end{bmatrix} \quad (1)$$

where, $\Gamma = \gamma(k_1 - k_2)/\ln(k_1/k_2)$

The first factorization on the left is irrotational orthogonal extension-contraction following the simple shear, the second factorization represents simple shear following the irrotational orthogonal extension-contraction, and the third expression is for transpression with simultaneous orthogonal extension-contraction

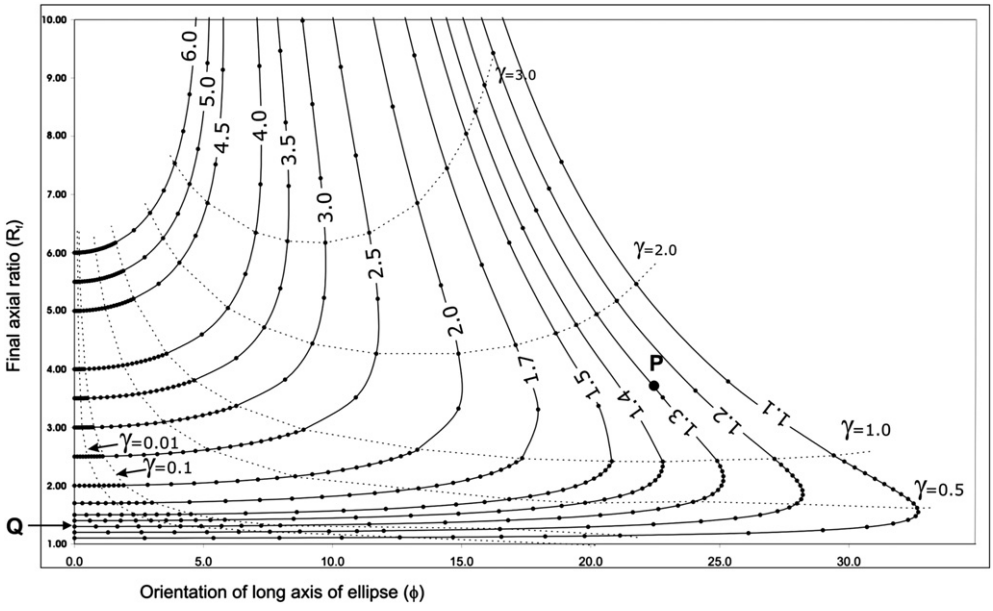

Fig. 7. Plot of the final axial ratio (R_f) against the orientation of the long axis of the ellipse (ϕ) defining a family of curves generated numerically with initial ellipses having different axial ratios (1.1–6.0) sheared by different values of γ (0.01–5.00). The solid lines represent the locus of the deforming ellipse of a fixed initial axial ratio for variable shear strains. The broken lines denote the contours of γ. Final ellipse P is unstrained to initial ellipse Q along the locus.

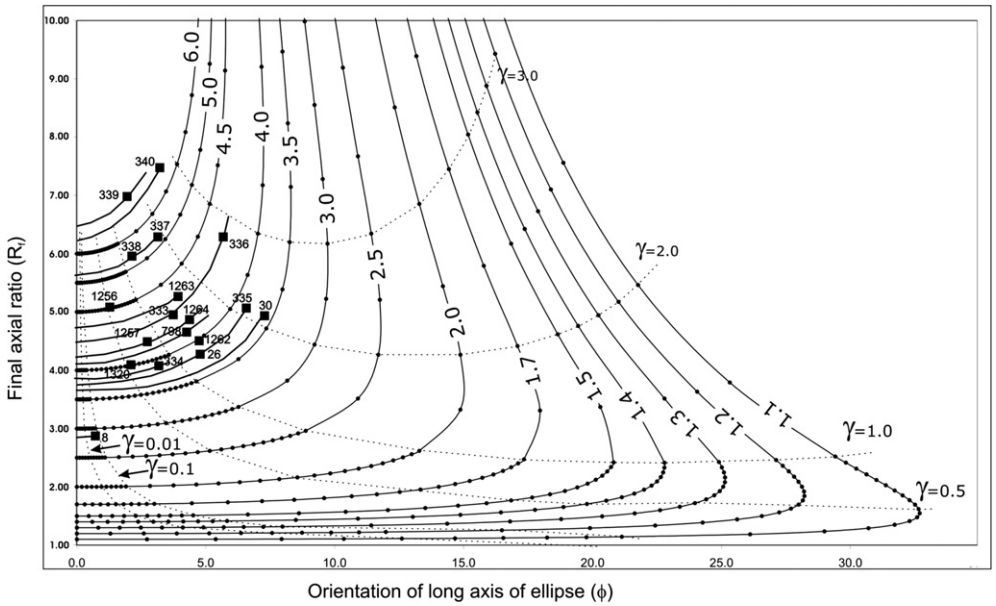

Fig. 8. Plots on Fig. 7 of the harmonic mean of axial ratio against the vector mean of the long axis orientation of the pebbles with respect to schistosity trace on the horizontal plane of measurement for different locations.

and simple shear. Γ may be called the effective shear strain in simultaneous simple shear and orthogonal extension-compression (transpression). The relation between the numerical values of shear strain in the simple shear component in the three cases is (Fossen and Tikoff, 1993),

$$\gamma_{p,s} = \Gamma/k_2 = \left(\gamma_{s,p}\right)(k_1/k_2) \quad (2)$$

It is obvious that, $\gamma_{p,s} > \Gamma > \gamma_{s,p}$ (3)

It is important to note that for the same finite strain the magnitude of the shear component is dependent on the order of superposition of pure and simple shear. However, the magnitude of the irrotational orthogonal extension-contraction (pure shear) component is the same in the three cases.

We have already discussed that in the present area the final structural pattern resulted from first irrotational orthogonal extension-contraction deformation (D_1) followed by horizontal simple shear. The pebble shapes observed are thus a result of these two episodes of deformation. The strong contraction and elongation associated with D_1 is evident from the appressed nature of the pebbles on the XZ section, where the long axes of the pebbles are aligned parallel to the schistosity trace. The horizontal dextral shear primarily modifies the shape and orientation of the pebbles on the horizontal (YZ) plane only and does not significantly alter the pebble shape on the vertical plane. Though strictly speaking the *Z*-direction of the final strain is not perpendicular to the schistosity, the difference is so small that for all practical purposes the vertical plane normal to the schistosity can be considered to be the XZ plane of the final finite strain as well as of the first strain.

6.1. Mathematical modeling of deformation with simple shear superimposed on compression

We have mathematically modeled the change of the shape of an initial ellipse by simple shear in a direction parallel to its long axis. In this model we consider that the initial orthogonal extension-contraction produced a strain ellipsoid whose longest axis (*X*) was vertical and intermediate and shortest axes were horizontal. On the horizontal surface the strain ellipse section (YZ) would have the long axis parallel to the trace of the schistosity. We chose a Cartesian coordinate system with abscissa (*x*-axis) parallel to the schistosity trace and the later simple shear has movement direction parallel to this axis (Fig. 6). Equations are derived to specify the orientation and axial ratio of the final strain ellipse for different values of γ and axial ratio of the initial ellipse (Appendix-A).

If the initial axial ratio($\sqrt{B/A}$) and γ are specified a family of curves can be drawn for a range of initial axial ratios depicting the values of the final axial ratio (R_f) and Φ at different γ values. Contours can be drawn for equal γ values. Such a family of curves has been generated by varying the initial axial ratio from1.1 to 6.0 and the γ-value from 0 (marking the initial values prior to deformation) to 5 (Fig. 7).

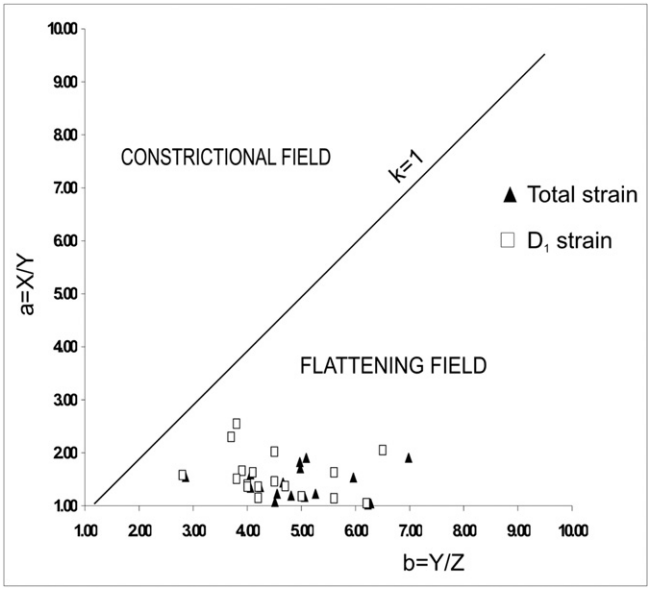

Fig. 9. Plot of D_1 strain ellipsoids final strain ellipsoids in Flinn plot.

It is observed that for ellipses which have a low value of initial axial ratio, ϕ increases rapidly with increasing γ until a critical value of γ is reached; the axial ratio increases very slightly at this stage. Beyond the critical value, ϕ starts to decrease, though at a slow rate and the axial ratio increases at a fast rate. There is a sharp inflection in the curve signifying change over from increasing ϕ to decreasing ϕ. With increase in the initial axial ratio the pattern remains the same but the inflection point in the curve becomes less pronounced. At high values of initial axial ratio there is no sharp inflection and ϕ increases at fast rate in the initial stage of deformation and at a very slow rate at higher values of γ. The axial ratio on the other hand increases slowly at the initial stage and very fast at the later stage; beyond $\gamma = 3.0$ the curves tend to become asymptotically parallel to the R_f axis.

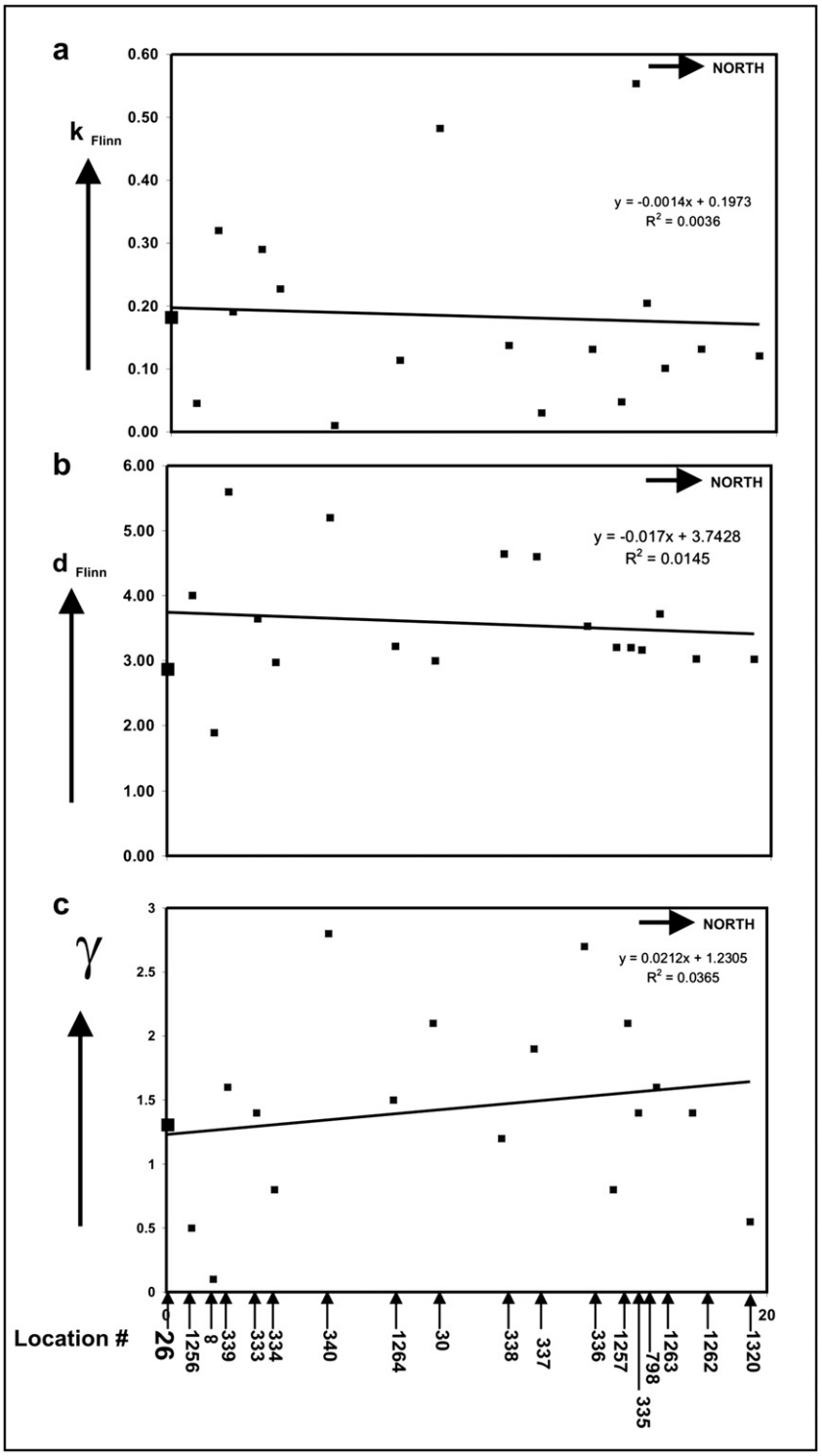

Fig. 10. Variation of (a) k, (b) d and (c) γ from north to south along the conglomerate band. On the abscissa distances of different locations from location 26 (southernmost station) are plotted.

Table 4
Different strain parameters calculated for the strain ellipsoid representing the initial extension-contraction strain (D_1) after taking away the effect of dextral simple shear, at different locations.

Location number	Axial ratio on the horizontal plane (Harmonic mean)	γ on the horizontal plane	Initial axial ratio (read off from the graph)	Axial ratio on the vertical plane (Harmonic mean)	*X*:*Y*:*Z*	*a* (X/Y)	*b* (Y/Z)	k_{Flinn}	d_{Flinn}
333	4.97	1.4	4.50	9.07	9.07:4.50:1	2.02	4.50	0.29	3.64
334	4.06	0.8	3.90	6.47	6.47:3.90:1	1.66	3.90	0.23	2.97
335	5.09	2.1	3.80	9.69	9.69:3.80:1	2.55	3.80	0.55	3.20
336	6.28	2.7	4.50	6.57	6.57:4.50:1	1.46	4.50	0.13	3.53
337	6.23	1.9	5.60	6.38	6.38:5.60:1	1.14	5.60	0.03	4.60
338	5.96	1.2	5.60	9.14	9.14:5.60:1	1.63	5.60	0.14	4.64
339	6.98	1.6	6.50	13.32	13.32:6.50:1	2.05	6.50	0.19	5.60
340	7.42	2.8	6.20	6.53	6.53:6.20:1	1.05	6.20	0.01	5.20
798	4.66	1.4	4.10	6.70	6.70:4.10:1	1.63	4.10	0.2	3.16
1256	5.06	0.5	5.00	5.91	5.91:5.00:1	1.18	5.00	0.05	4.00
1257	4.51	0.8	4.20	4.84	4.84:4.20:1	1.15	4.20	0.05	3.20
1262	4.55	1.4	4.00	5.58	5.58:4.00:1	1.4	4.00	0.13	3.03
1263	5.26	1.6	4.70	6.46	6.46:4.70:1	1.37	4.70	0.1	3.72
1264	4.81	1.5	4.20	5.73	5.73:4.20:1	1.36	4.20	0.11	3.22
1320	4.06	0.55	4.00	5.45	5.45:4.00:1	1.36	4.00	0.12	3.02
8	2.86	0.1	2.80	4.42	4.42:2.80:1	1.58	2.80	0.32	1.89
26	4.24	1.3	3.80	5.74	5.74:3.80:1	1.51	3.80	0.18	2.85
30	4.98	2.1	3.70	8.52	8.52:3.70:1	2.3	3.70	0.48	3.00

The usefulness of these curves lies in the fact that any measured ellipse can be plotted on the graph and the amount of the shear strain can be directly read off from its position in the plot. Moreover we can unstrain the ellipse along its trajectory and determine the value of the initial axial ratio, when $\phi = 0$, and $\gamma = 0$.

For example, consider a point 'P' (Fig. 7) for an ellipse with a final axial ratio (R_f) of 3.65 whose long axis is oriented at an angle of 22.5° with the *x*-direction (ϕ). On unstraining along its trajectory, the orientation of the long axis of the ellipse would increase from 22.5° to 25° and then gradually decrease to 0° when it reaches the y-coordinate axis at 'Q'. The point 'Q' marks the initial axial ratio (R_i) of the ellipse prior to shear deformation, which is 1.3.

The measured pebble data for the YZ section have been plotted on this graph (Fig. 8). In all but two locations the graphically calculated γ values (Table 4) fall within the range of 0.5–2.8 (with a mean value of 1.43) and the initial axial ratio (Y:Z of the strain ellipsoid of D_1 deformation)varies from 3.7 to 6.5 (with a mean value of 4.61). This initial axial ratio is due to the irrotational orthogonal extension-contraction associated with D_1. Only at one location (No. 8) γ has a very low value of 0.1, and the corresponding initial axial ratio is 2.8. This value is far from the main cluster of the plots (Fig. 8). It follows from Eq. (3) that the effective shear strain would have been less if the same finite strain resulted from simultaneous simple shear and orthogonal extension-contraction (transpression). This would have no effect on the computed magnitude of the orthogonal extension-contraction. (Fossen and Tikoff, 1993; Tikoff and Fossen, 1993)

6.2. Calculation of 3-d strain ellipsoid after the D_1 extension-contraction strain

The horizontal shear does not significantly change the axial ratio on the vertical (XZ) plane. Hence the measured ratio can be taken to represent the X:Z ratio of the D_1 strain ellipsoid. If the initial axial ratio determined from Fig. 8 assumes a value ***m : 1*** on the horizontal plane (YZ plane) and the strain ratio computed (vide Tables 1 and 3) on the vertical plane(XZ plane) be ***n : 1***, then the 3-d strain ellipsoid has an axial ratio of ***n : m : 1***. The 3-d strain ratios have been calculated for each location. These reflect the 3-d geometry of the initial D_1 strain. The results are listed in Table 4.

On plotting of these ellipsoids on the Flinn Diagram (Fig. 9) it is observed that all of them lie in the flattening field close to the line of pure oblate ellipsoids. The *k*-values (Flinn, 1962), which are indicators to the shapes of the ellipsoids, are consistently less than 1 and are more or less constant (Fig. 10a). The *k*-values range from 0.01 to 0.55, most of them being less than 0.20. The finite strain geometry is analogous to that for Type C transpression of Fossen and Tikoff (1998) with equal stretching in two directions perpendicular to shortening, that is, equal stretching in the vertical direction and in the shear direction. The measure of the intensity of deformation, *d*, (Ramsay and Huber, 1983) is extremely variable in the regions south of Barr village (Fig. 10b). North of it *d*-values vary from 3.02 to 4.64. Most of the γ values fall within the range 0.5–2.8 (Fig. 10c). There is no spatial control on the values of the above three parameters. Fig. 10 shows that the values are uncorrelated with the distance from a reference point. The correlation coefficient values (r) are 0.06–0.19, which are not significant at 90% confidence level. Hence strain measurements clearly indicate that though on outcrop scale the strain is broadly homogeneous, on a regional scale there is strain heterogeneity.

7. Conclusions

The pebble shapes in Barr Conglomerate have resulted from an earlier irrotational orthogonal extension-contraction strain followed by horizontal dextral simple shear. The procedure of factorizing the total strain into the two components has been discussed. The computations indicate quite a high value of shear strain (mean value of 1.43). This is consistent with the interpretation of the earlier workers about the presence of a shear zone along the western contact of the South Delhi Fold Belt. Though the strain appears to be homogeneous in the scale of an outcrop there is considerable strain heterogeneity on a regional scale. However, there is no systematic spatial variation of the strain parameters. The total strain as well as the earlier orthogonal extension-contraction strain is of flattening type. Had the deformation been of transpression type with simultaneous pure shear and simple shear the magnitude of the simple shear component would have been less than our computed value; the extension-contraction magnitude would have remained the same.

Acknowledgments

A part of the research was funded by the Department of Science and Technology, Government of India through the sanction of a Research Project to D.M. N.D is grateful to the University Grants

Commission for sanction of research grants for this work. We are grateful to the Heads of the Departments of Geology of the University of Calcutta and the Presidency College for providing the necessary infrastructural facilities. We have been greatly benefited by the constructive reviews of Professor Richard Lisle and Professor Peter Hudleston. We also thank Prof. Holdsworth for his editorial advice and taking keen interest in the paper.

Appendix A

Let the equation of the initial ellipse (Fig. 6) after D_1 deformation be,

$$Ax^2 + By^2 = 1 \tag{A1}$$

The axial ratio of the ellipse would be $\sqrt{(B/A)}$.

Subsequently this ellipse is deformed by dextral simple shear (γ taken to be positive) with displacement on the schistosity surface in the direction parallel to x-coordinate axis. The transformation equation representing this simple shear is:

$$x' = x + \gamma y \tag{A2}$$

$$y' = y \tag{A3}$$

Hence for Eqs. (A2) and (A3) we can write:

$$x = x' - \gamma y' \tag{A4}$$

$$y = y' \tag{A5}$$

The ellipse of Eq. (A1) would be transformed to a figure given by :

$$A\left(x' - \gamma y'\right)^2 + B\left(y'\right)^2 = 1 \tag{A6}$$

Expanding:

$$A\left(x'\right)^2 - 2A\gamma x'y' + \left(A\gamma^2 + B\right)\left(y'\right)^2 = 1 \tag{A7}$$

The Eq. (A7) is an equation of an ellipse with the form of :

$$Px^2 + 2hxy + Qy^2 = 1 \tag{A8}$$

Where,

$$P = A;\ h = -A\gamma;\ Q = \left(A\gamma^2 + B\right)$$

It is to be remembered that the fraction $\sqrt{(B/A)}$ is the measure of the axial ratio of the initial ellipse.

The lengths of the semi axis of the final ellipse can be found out by solving the characteristic equation (Ghosh, 1993; pp. 141–142).

$$S^2 - I_1 S + I_2 = 0 \tag{A9}$$

where two invariants I_1 and I_2 are given by the equations:

$$I_1 = P + Q = A + A\gamma^2 + B \tag{A10}$$

$$I_2 = PQ - h^2 = A\left(A\gamma^2 + B\right) - (-A\gamma)^2 \tag{A11}$$

The roots of the Eq. (A9) are the two principal axes of the ellipse, given by:

$$s_1 = \frac{1}{2}(P + Q) + \frac{1}{2}\sqrt{(P - Q)^2 + 4h^2} \tag{A12}$$

and

$$s_2 = \frac{1}{2}(P + Q) - \frac{1}{2}\sqrt{(P - Q)^2 + 4h^2} \tag{A13}$$

Replacing the values of P, Q and h in Eqs. (A12) and (A13) in terms of A, B and γ we get:

$$s_1 = \frac{1}{2}\left(A + A\gamma^2 + B\right) + \frac{1}{2}\sqrt{\left(A - A\cdot\gamma^2 - B\right)^2 + 4(-A\gamma)^2} \tag{A14}$$

and

$$s_2 = \frac{1}{2}\left(\mathrm{A} + \mathrm{A}\gamma^2 + \mathrm{B}\right) - \frac{1}{2}\sqrt{\left(A - A\cdot\gamma^2 - B\right)^2 + 4(-A\gamma)^2} \tag{A15}$$

The axial ratio of the deformed ellipse is given by

$$R_f = \frac{s_1}{s_2} \tag{A16}$$

The orientation of the long axis of the deformed ellipse is given by the equation:

$$\tan(2\phi) = \frac{2h}{P - Q} \tag{A17}$$

where ϕ is the angle between the long axis of the deformed ellipse with the x-coordinate axis (Fig. 6). Substituting P, Q and h in terms of A, B and γ, we get:

$$\tan(2\phi) = \frac{2(-A\gamma)}{A - A\gamma^2 - B} \tag{A18}$$

It is thus seen that the Eqs. (A16) and (A18) constrain the shape and the orientation of the final strain ellipse that results from simple shear superimposed on an initial strain with principal stretches parallel and perpendicular to the shear plane (Fig. 6).

Appendix. Supplementary material

Supplementary material associated with this article can be found, in the online version, at doi:10.1016/j.jsg.2011.10.010.

References

Bilby, B.A., Eshelby, J.D., Kundu, A.K., 1975. The change in shape of a viscous ellipsoidal region embedded in a slowly deforming matrix having a different viscosity. Tectonophysics 28, 265–274.

Dasgupta, N., 2010. Structural Geometry and Strain pattern in the rocks of the Delhi Fold belt in an area near Barr, Pali District, Central Rajasthan. Unpublished Ph.D. thesis, University of Calcutta.

De Paor, D.G., 1988. R_f/φ strain analysis using an orientation net. Journal of Structural Geology 10, 323–333.

Dunnet, D., 1969. A technique of finite strain analysis using elliptical particles. Tectonophysics 7, 117–136.

Dunnet, D., Siddans, A.W.B., 1971. Non-random sedimentary fabrics and their modification by strain. Tectonophysics 12, 307–325.

Elliott, D., 1970. Determination of finite shape and initial shape from deformed elliptical objects. Bulletin Geological Society of America 86, 2221–2236.

Flinn, D., 1962. On folding during three-dimensional progressive deformation. Quarterly Journal of Geological Society, London 118, 385–433.

Fossen, H., Tikoff, 1993. The deformation matrix for simultaneous simple shearing, pure shearing and volume change, and its application to transpression-transtension tectonics. Journal of Structural Geology 15, 413–422.

Fossen, H., Tikoff, 1998. Extended models of transpression and transtension, and application to tectonic settings. In: Holdsworth, R.E., Strachan, R.A., Dewey, J.F. (Eds.), Continental Transpressional and Transtensional Tectonics, vol. 135. Geological Society, London, pp. 15–33. Special Publications.

Freeman, B., 1987. The behaviour of deformable ellipsoidal particles in three-dimensional slow flows: implications for geological strain analysis. Tectonophysics 132 (Issue 4), 297–309.

Gardner, M., 1965. The superellipse: a curve that lies between the ellipse and the rectangle. Scientific American 21, 222–234.

Gay, N.C., 1968a. Pure shear and simple shear deformation of inhomogeneous viscous fluids: theory. Tectonophysics 5, 211–234.

Gay, N.C., 1968b. Pure shear and simple shear deformation of inhomogeneous viscous fluids: Pt. II: the determination of total finite strain in a rock from objects such as deformed pebbles. Tectonophysics 5, 295–302.
Gay, N.C., 1969. Analysis of strain in the Barberton Mountain Land, eastern Transvaal, using deformed pebbles. Journal of Geology 77, 377–396.
Gay, N.C., Fripp, R.E.P., 1976. The control of ductility on the deformation of pebbles and conglomerates. Philosophical Transactions Royal Society London A 283, 109–128.
Ghosh, S.K., Hazra, S., Sengupta, S., 1999. Planar, non-planar and refolded sheath folds in the Phulad Shear Zone, Rajasthan, India. Journal of Structural Geology 21, 1715–1729.
Ghosh, S.K., 1993. Structural Geology: Fundamentals and Modern Developments. Pergamon Press, New York.
Gupta, P., Bose, U., 2000. An Update of the Geology of the Delhi Supergroup in Rajasthan, vol. 55. Geological Survey of India. Special Publication287–306.
Heron, A.M., 1953. The geology of Central Rajputana. Memoir, Geological Survey of India 79.
Holst, T.B., 1982. The role of initial fabric on strain determination from deformed ellipsoidal objects. Tectonophysics 82, 329–350.
Lisle, R.J., 1977. Estimation of the tectonic strain ratio from the mean shape of deformed elliptical markers. Geologie en Mijnbouw 56, 140–144.
Lisle, R.J., 1985. Geological Strain Analysis: A Manual for the R_f–Φ Method. Pergamon Press.
Lisle, R.J., 1988. The superellipsoidal form of coarse clastic sediment particles. Mathematical Geology 20, 879–890.
Mandal, N.K., Samanta, S.K., Bhattacharyya, G., Chakraborty, C., 2003. Deformation of ductile inclusions in a multiple inclusion system in pure shear. Journal of Structural Geology 25, 1359–1370.
Mukhopadhyay, D., Bhattacharya, S., 1969. A study of the pebble deformation in the Precambrian rocks of the Singhbhum district, Bihar. Journal Geological Society of India 10, 77–87.
Mukhopadhyay, D., 1973. Strain measurements of deformed quartz grains in the slaty rocks from the Ardenees and the northern Eifel. Tectonophysics 16, 279–296.
Oertel, G., 1978. Strain determination from the measurement of pebble shapes. Tectonophysics 50, 73–78.
Ramsay, J.G., 1967. Folding and Fracturing of Rocks. McGraw Hill, New.York.
Ramsay, J.G., Huber, M.I., 1983. The Techniques of Modern Structural Geology, vol. 1. Academic Press, London.
Shimamoto, T., Ikeda, Y., 1976. A simple algebraic method for strain estimation from deformed ellipsoidal objects. 1. Basic Theory. Tectonophysics 36, 315–337.
Sengupta, S., Ghosh, S.K., 2004. Analysis of transpressional deformation from geometrical evolution of mesoscopic structures from Phulad shear zone, Rajasthan India. Journal of Structural Geology 26, 1961–1976.
Sengupta, S., Ghosh, S.K., 2007. Origin of striping lineation and transposition of linear structures in shear zones. Journal of Structural Geology 29, 273–287.
Sen, S., 1980. Precambrian stratigraphic sequence in a part of the Aravalli range, Rajasthan: a re-evaluation. Quarterly Journal of the Geological Mineralogical Metallurgical Society of India 52 (2), 67–76.
Sen, S., 1981. Proterozoic paleotectonics in the evolution of crust and location of metalliferrous deposits, Rajasthan. Quarterly Journal of the Geological, Mineralogical and Metallurgical Society of India 53, 162–185.
Tikoff, B., Fossen, H., 1993. Simultaneous pure and simple shear: the unifying deformation matrix. Tectonophysics 217, 267–283.
Treagus, S.H., Lan, L., 2000. Pure shear deformation of square objects, and applications to geological strain analysis. Journal of Structural Geology 22, 105–122.
Treagus, S.H., Lan, L., 2003. Simple shear of deformable square objects. Journal of Structural Geology 25, 1993–2003.
Treagus, S.H., Lan, L., 2004. Deformation of square objects and boudins. Journal of Structural Geology 26, 1361–1376.
Treagus, S.H., Treagus, J.E., 2001. Effects of object ellipticity on strain, and implications for clast–matrix rocks. Journal of Structural Geology 23, 601–608.
Vitale, S., Mazzoli, S., 2005. Influence of object concentration on finite strain and effective viscosity contrast: insights from naturally deformed packstones. Journal of Structural Geology 27, 2135–2149.
Wheeler, J., 1984. A new plot to display the strain of elliptical markers. Journal of Structural Geology 6, 417–423.